STP 1637, 2022 / available online at www.astm.org / doi: 10.1520/STP163720200109

Joseph Reid Carazzone[1]

Aspects of Sinter-Cracking in Binder Jet 3D Printed Parts

Citation

J. R. Carazzone, "Aspects of Sinter-Cracking in Binder Jet 3D Printed Parts," in *Progress in Additive Manufacturing 2020*, ed. N. Shamsaei and M. Seifi (West Conshohocken, PA: ASTM International, 2022), 92–104. http://doi.org/10.1520/STP163720200109[2]

ABSTRACT

Binder jet three-dimensional (3D) printing is a scalable, potentially low-cost additive manufacturing route able to process materials not attainable to other techniques, especially nonweldable materials. It relies on postprocess sintering to achieve final properties but encounters problems with distortion and cracking during sintering. The present work seeks to understand how part design geometry and 3D printing build orientation influence cracking during sintering, with the goal of mitigating the problem. In situ monitoring experiments reveal how sinter-cracks initiate and grow in 3D-printed notched panel specimens during densification. Different design geometries and build directions are tested to identify sinter-crack-resistant regimes.

Keywords

sintering, cracking, binder jet, 3D printing, in situ monitoring

Introduction

Binder jet three-dimensional (3D) printing is an additive manufacturing method that works by consolidating layers of powder material using a heat-cured liquid adhesive.[1] It can process most flowable powder materials, including nonweldable

Manuscript received December 2, 2020; accepted for publication March 5, 2021.

[1]Dept. of Materials Science and Nanoengineering, 6100 Main St., MS 325, Rice University, Houston, TX 77005, USA https://orcid.org/0000-0003-2387-2349

[2]ASTM *International Conference on Additive Manufacturing* held virtually on November 16–20, 2020.

ones. As a low-temperature process, it avoids problems associated with focused energy beam methods, such as nonequilibrium phases and large thermal gradients. The strength of the printed part is developed during postprocess sintering, when the adhesive burns out and the powder material bonds and densifies.

Sintering bonds and densifies a powder material at temperatures around 90% of the material melting point. By controlling the temperature schedule, precise control of microstructural evolution can be achieved.[2] For a binder jet printed material, the loosely packed powder can experience linear shrinkages as high as 20% during densification. Such large shrinkages tend to cause self-induced stress; when combined with factors such as interfacial friction or packing inhomogeneity, such stress can lead to cracking.[3,4] This problem, termed *sinter-cracking*, takes on new meaning with the complex geometries and mesostructures encountered in binder jet 3D printed parts.

Recently, a method was demonstrated for investigating sinter-cracking in binder jet parts through in situ monitoring, allowing instantaneous measurement of densification and crack growth.[5] The objective of the present work is to use the method to probe variables that may influence sinter-crack initiation and growth: the geometry of a 3D printed design feature and the orientation of the 3D object during printing.

Regarding design geometry, past investigations have considered stress-raising features such as blunt notches[6] or sharp cracks[4] as crack nucleation sites, using either the stress concentration or stress intensity factors to quantify the results. However, there is still a need for a fuller picture of how the size and shape of a negative design feature influences sinter-crack initiation and growth, particularly in binder jet printed materials. Regarding build orientation, anisotropic material properties are known issues for additively manufactured materials.[7] In binder jet, the printed part may be oriented freely within the build box, with the build direction assuming an arbitrary orientation with respect to the part design. Typically, the build direction represents the weakest dimension of the printed material because the material bonds between build layers are weaker than the material bonds within the build layers. Thus, anisotropic sinter-cracking behavior is expected based on the orientation of the sinter-crack initiation site with respect to the build direction.

In this work, the effects of both design geometry and build orientation on sinter-cracking in binder jet parts will be probed using center-notched tension panel specimens and in situ monitoring experiments, with the goal of identifying factors that tend to mitigate initiation and growth of sinter-cracks.

Materials and Methods

SAMPLE PREPARATION

Center-notched tension panel specimens were fabricated on an ExOne Innovent binder jet 3D printer according to the design shown in figure 1, with the dimensions of 34 by 9 mm and a gage thickness of 2 mm. The binder was a proprietary aqueous

FIG. 1 (*A*) Front profile of the notched panel specimen placed in the stainless steel restraining fixture. The open slot at the top prevents stress buildup due to thermal expansion. (*B*) Side profile of the specimen and fixture.

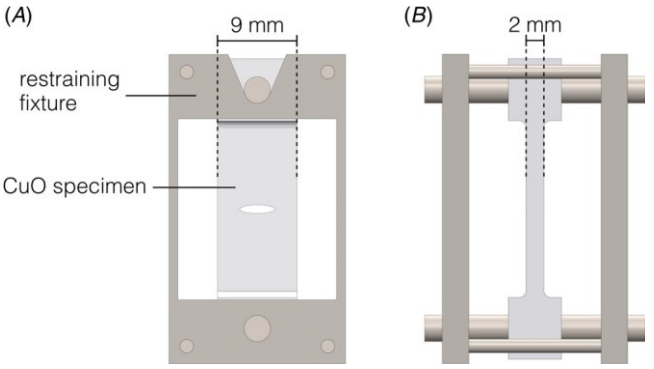

solution based on ethylene glycol;* the binder saturation level† was 100%, and the layer thickness was 80 1m. Curing of the binder occurred at 60°C during the print and 200°C afterward. The powder material used was technical grade cupric oxide of −200 mesh particle size.‡

Variation of Notch Geometry

Specimens were designed with small and large circular notches of diameters 0.70 and 3.8 mm, and small and large elliptical notches of major and minor axes 0.70 by 0.30 mm and 3.8 by 0.70 mm. A specimen with no notch was also prepared as a control. The notch geometries correspond to gross stress concentration factors (K_{tg}) of 3.0 and 3.8 for the small and large circular notches, and 5.7 and 13.9 for the elliptical notches, respectively.[8] The minimum section of each, calculated as the specimen width less the notch width, normalized by the specimen width, was 0.9 and 0.6 for the samples with small and large notches, respectively.

Variation of Build Direction

A specimen was designed with an elliptical notch with the dimensions 2.90 by 0.40 mm (K_{tg} ¼ 16.9). Samples were printed in the three orthogonal build orientations illustrated in figure 2. The crack arrester configuration has build layers perpendicular to the notch and parallel to the restraint; the crack divider has build layers

*7100037CL, ExOne, North Huntingdon, PA.
†The binder saturation level is based on the estimated powder packing density and is defined as the volume of applied binder normalized by the volume of porosity in the powder bed.[1]
‡CU-601, Atlantic Equipment Engineers, Upper Saddle River, NJ.

FIG. 2 (*A*) Orientation of samples in the build box. The axes indicate the build direction as well as the directions of recoater and printhead travel. (*B*) Cross-sectional views of the samples showing orientation of the build layers with respect to the notch, indicated by overlaid black lines: (1) crack arrester, (2) crack divider, and (3) short transverse geometries.

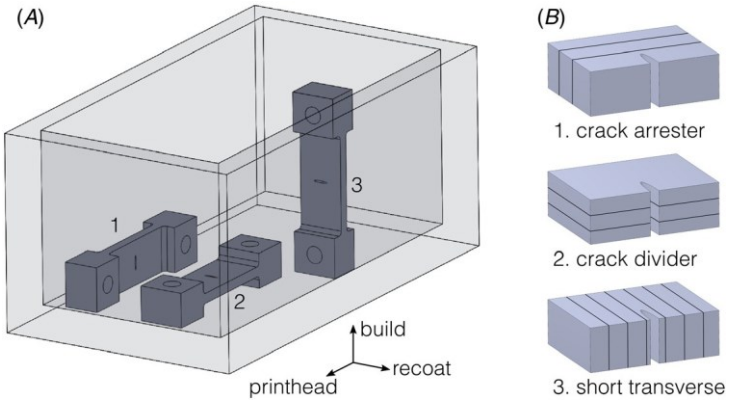

parallel to the notch and to the restraint; and the short transverse has build layers parallel to the notch and perpendicular to the restraint.

IN SITU MONITORING EXPERIMENTS

Samples were held in a stainless steel fixture, as shown in figure 1. The resulting restraint prevents vertical shrinkage of the sample, promoting a uniaxial stress state. The apparatus was placed in the center of a tube furnace with a plug on one end. The system was brought to 1,000°C (80% of the sample material melting point) with a maximum heating rate of 10°C/min, then held for 10 to 15 h. Samples were photographed at 5-s intervals with a 22.3 megapixel DSLR camera equipped with a 200-mm lens and 2x extender.

IMAGE ANALYSIS

Image analysis was performed with the Fiji platform,[9] using binary thresholding with particle and point analysis to determine instantaneous relative density and crack length. Measurement of the relative density (q) was determined by equation (1):

$$q = q_0 \left(\frac{A_0}{A}\right)^2 \quad (1)$$

where:

A = projected sample area measured from the images.

The initial relative density, $q_o = 0.36$, was determined by the mass and volume of a cylindrical sample specimen printed under similar conditions. The equation

assumes isotropic horizontal shrinkage with no change in the height of the sample. Crack length (*a*) was determined from image analysis as the horizontal distance from the original notch root to the tip of the continuous crack emanating from it, taking into account movement of the original notch root due to sample shrinkage.

Results and Discussion

VARIATION OF NOTCH GEOMETRY

Photographs of the samples before and after 10 h of sintering are shown in figure 3. Horizontal shrinkage in each case reveals densification in the unrestrained dimensions. The control sample shows no cracking. In the notched samples, the vertical restraint has caused varying degrees of distortion and damage. The small notches experience vertical opening and slight horizontal narrowing but show no cracking. The large circular notch shows vertical opening and horizontal narrowing as well as inward tapering of the sides adjacent to the notch. A small crack initiated near one notch root and propagated slightly. The large elliptical notch shows signs of vertical opening as well as tapering of the sides. Cracks initiated near both notch roots and propagated through the material, causing complete fracture. The fracture surface is rough, indicative of the ductile rupture behavior previously observed in sinter-cracking.[4,5,10]

In the case of both large notches, it is evident that the samples experienced a self-induced stress arising from constrained densification. The material attempts to shrink in all directions uniformly but is prevented in the direction of restraint, leading to a tensile stress that ultimately arises from the surface energy of the material. This stress state is revealed in both the pronounced shape distortion of the circular notch sample and the rupture of the elliptical notch sample. In both cases, concentration of the self-induced stress by the notch has led to the observed damage.[3,11]

FIG. 3 In situ images of samples prior to (top row) and after (bottom row) 10 h of densification. (*A*) Control sample with no notch. (*B*–*E*) Notched samples possessing K_{tg} of 3.0, 5.7, 3.8, and 13.9, respectively. Scale bars are 2 mm.

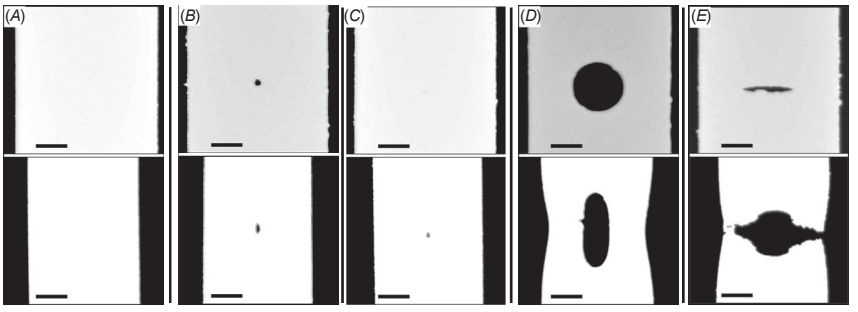

Figure 4 gives the measurements of instantaneous relative density for each sample during sintering. The graph reveals the onset of densification occurring at 900°C, followed by an acceleration as the temperature reaches the 1,000°C isotherm, passing through a maximum densification rate of ~ 0.17 hr^{-1}. After this point, densification slows down to a steady rate, and differences emerge between the samples. Generally, for notches with greater K_{tg}, densification is faster. The material above and below the notch is not fully restrained and is able to densify with a vertical component of motion. For the large elliptical notch, propagation of the crack creates new surfaces, further decreasing the restraint. The result is increased specimen compliance, caused by surfaces in the notch and subsequent cracks that extend transverse to the loading axis.[11,12] The sample geometries with a lower minimum section possess higher compliance, allowing a greater vertical component to shrinkage and thus faster densification.

Surrounding the notch, the densifying material experiences varying degrees of restraint on its densification. For the large notches in particular, this variation leads to anisotropic evolution of the specimen relative density, which is not captured

FIG. 4 Relative density versus time as measured from the in situ images. Sample geometries are indicated by K_{tg} next to each curve (the control is represented as 1.0). The temperature profile (T) is shown above.

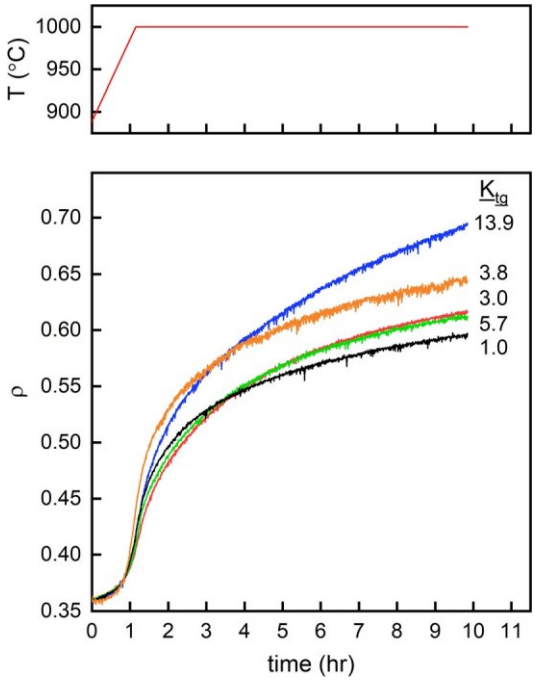

by equation (1). In previous work, this anisotropy was tested through image analysis of a micrograph of a polished specimen cross section.[5] The analysis revealed an average relative density around the notch that agreed with the value obtained from the in situ photographs. However, differences were noted in local regions, with material above and below the notch exhibiting greater relative density and material around the crack exhibiting lower relative density.

The state of uniaxial restraint imposed on the densifying specimen produces a self-induced stress in the material.[11] The concentration of this stress around the notch leads to initiation and growth of cracks from the notch roots, as illustrated by the inset of figure 5. Microstructural details of the sinter-crack initiation and growth process have been given in previous work.[5]

No measurable cracking was observed for the samples with no notch and with small notches of K_{tg} ¼ 3.0 and 5.7, (minimum section ¼ 0.9). Figure 5 plots evolution of a versus q in the samples with large notches (K_{tg} ¼ 3.8 and 13.9, minimum section ¼ 0.6). In both cases, crack initiation follows an initial incubation period of densification. For the elliptical notch, initiation begins after a change in q of 0.13. Propagation occurs at an average growth rate (a_) of 0.28 mm/h, interrupted by brief periods of crack arrest or diminished growth. Complete fracture occurs after a further increase of q by 0.17. For the circular notch, cracking begins after q increases by 0.25, followed by more uniform propagation with a_ ¼ 0.07 mm/h.

FIG. 5 Crack length versus relative density for the large circular (K_{tg} ¼ 3.8) and large elliptical (K_{tg} ¼ 13.9) notches, as measured from the in situ images. The X indicates the point of complete fracture.

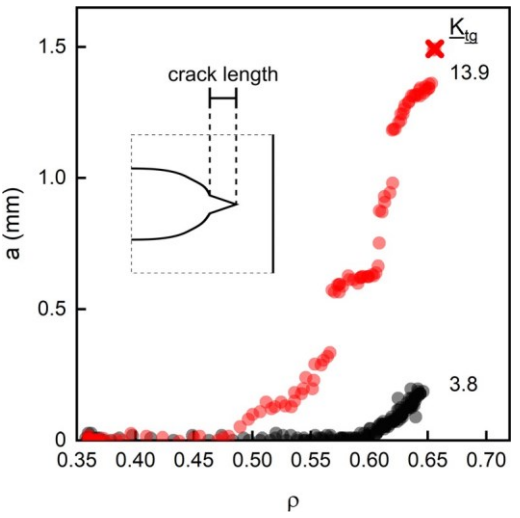

In both cases, crack propagation is gradual, and failure does not occur instantaneously.

The absence of cracking in the samples with small notches (large minimum section) is consistent with previous theoretical predictions based on stress intensity analysis of a thin crack in a constrained sintering film.[13] Initiation of crack growth was predicted to not occur when the initial crack length falls below a critical value; this was further confirmed experimentally for sintering films.[4] The present results suggest that the same is true for binder jet printed materials containing negative design features (i.e., that there is a critical feature size below which sinter-crack initiation will not occur).

The difference in crack initiation between the small and large notches highlights the importance of flaw size in sinter-cracking; the difference in crack initiation and propagation between the large circular and elliptical notches highlights the importance of flaw shape. The crack initiation period for the large circular notch was twice that of the large elliptical notch, while the crack growth rate was less by a factor of four. Thus, when the notch is large enough to cause crack initiation, then the shape of the notch plays a role in the time of that initiation and the subsequent growth rate.

It is helpful to consider creep-cracking in fully dense materials, a phenomenon similar to sinter-cracking.[4,10] Hayhurst, Morrison, and Leckie determined that it was the average stress acting on the minimum section, not the stress due to the elastic stress concentration factor, that governs the creep rupture time in fully dense copper and aluminum center-notched panels.[14] For sinter-cracking, the present results show similarities and differences. For crack initiation, the notch size threshold is independent of the notch stress concentration factor: the small elliptical notch (K_{tg} ¼ 5.7) had a larger stress concentration factor than did the large circular notch (K_{tg} ¼ 3.8), yet it did not initiate cracking. When the notch is large enough to initiate a crack, then both initiation and growth depend on the stress concentration factor: the large elliptical notch (K_{tg} ¼ 13.9) experienced earlier crack initiation and faster crack growth than did the large circular notch. Therefore, sinter-cracking is similar to linear elastic fracture mechanics in these ways: existence of a critical flaw size and dependence on the flaw stress concentration factor.[13,15]

It is likely that the critical flaw size observed here corresponds to a critical minimum section, as observed by Hayhurst, Morrison, and Leckie.[14] Therefore, to avoid cracking during sintering of binder jet printed parts, it is suggested that negative design features remain above a critical minimum section. If the critical minimum section must be exceeded, then minimization of the feature's stress concentration factor may prevent sinter-crack initiation. Following the observed delay in crack initiation for the large circular notch, minimizing the amount of densification required could also prevent cracking. This could be achieved by increasing the relative density of the binder jet parts prior to sintering, such as through using a powder material with a polymodal particle size distribution, or through infiltrating a partly sintered part with solid material precursors.[16]

VARIATION OF BUILD ORIENTATION

The results of sinter-cracking in the samples prepared with different build orientations are shown in the images of figure 6. The initial notch geometry (a large ellipse with K_{tg} ¼ 16.9) is shown along with each build orientation at the end of sinter-cracking: images were selected at the point of complete fracture of one side of the sample or at the end of 15 h of densification. In all cases, the initially sharp notch led to significant cracking. The crack arrester configuration (fig. 6*B*) experienced a tortuous crack path, very rough fracture surface, and a vertical component in the path of crack propagation. It remained intact after 15 h of densification. The spacing of rough features on the fracture surface, visible in figure 6*B*, corresponds in several instances to the thickness of the binder jet build layers, which lie perpendicular to the specimen face. The crack divider configuration (fig. 6*C*) underwent complete fracture of one side after 0.6 h of densification. It experienced a direct crack path proceeding horizontally from the notch, with cracking mainly occurring on one side of the specimen. The short transverse configuration (fig. 6*D*) experienced the most extensive cracking, undergoing nearly simultaneous fracture of both sides after 3 h of densification, with mainly horizontal crack paths. The roughness in the specimen sides arose from separation of the build layers.

Evolution of sinter-crack length in the build orientation samples is plotted versus relative density in figure 7, where the fastest growing crack is represented for each sample. The crack divider and short transverse samples both begin cracking early, after an increase in q of ~ 0.03. Both experience arrest phases around a ¼ 0.5 mm, where the crack length decreases slightly. The crack divider sample

FIG. 6 In situ images of sinter-crack evolution in the build orientation samples: (*A*) notch geometry prior to densification; (*B*) crack arrester; (*C*) crack divider; and (*D*) short transverse build orientations. The times elapsed from the onset of densification until the end of experiment shown in (*B*), (*C*), and (*D*) are 15, 2, and 4 h, respectively. Scale bars are 2 mm.

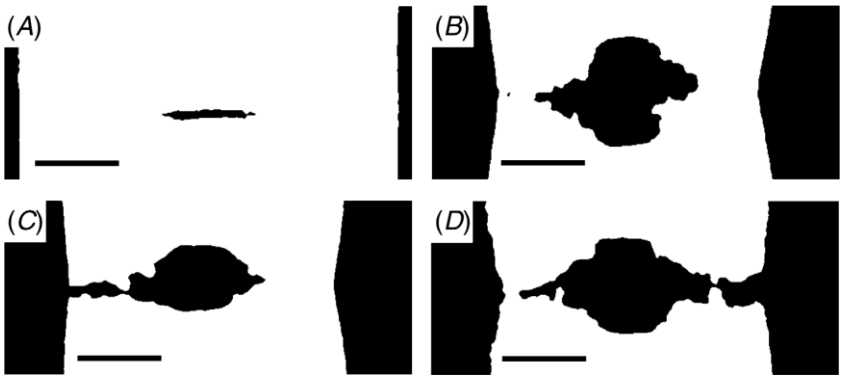

FIG. 7 Crack length versus relative density for the different build orientations: crack divider, short transverse, and crack arrester. The X symbol indicates the point of complete rupture.

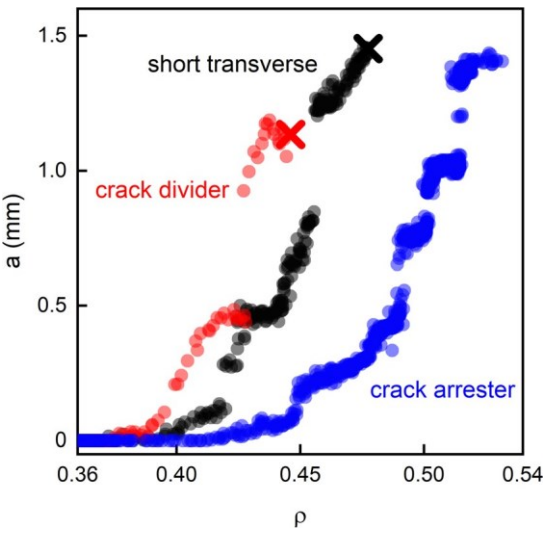

experiences an average $\dot{a}$ of 1.9 mm/h and ruptures at $a \approx 1.2$ mm and $q \approx 0.45$. The short transverse sample experiences slower cracking, with $\dot{a} \approx 0.5$ mm/h and reaches a slightly greater final crack length and relative density, rupturing at $a \approx 1.5$ mm and $q \approx 0.48$. The crack arrester sample experiences the longest incubation period, beginning to crack after an increase in q of ~ 0.05. It experiences several crack arrest phases in which the crack continues to grow slightly; its average $\dot{a}$ is 0.1 mm/h, and the sample attains a final q of 0.53 without complete rupture.

The different behaviors observed in figures 6 and 7 are in line with those understood for fully dense materials possessing a laminate layer structure, such as rolled steels. According to Hertzberg,[15] the short transverse configuration is expected to be the weakest, with no toughening mechanisms available to it: the tensile stress acts normal to the weak interfaces between the layers while the crack propagates along them, minimizing fracture toughness. The crack divider, however, has an available toughening mechanism: the tensile stress acts in the plane of each layer rather than acting normal to the weak interfaces. Thus, each layer acts as a thin material sheet in which a planar stress state exists, which reduces stress triaxiality and increases fracture toughness.

The toughening mechanism for the crack arrester arises from the propagation of the crack normal to the layer interfaces, which causes interface delamination ahead of the crack. This delamination blunts the crack tip, reduces stress triaxiality, and can lead to crack deflection, all increasing fracture toughness. Operation of this

mechanism is suggested in figure 6*B* by the multiple pronounced ligaments on the fracture surface and the vertical component of crack propagation in the crack arrester sample. In a similar consideration, the same mechanism could operate with the layered mesostructure that arises from the application of binder droplets during printing, appearing as rows of densely packed material separated by less dense interfaces within the build layer. Delamination of these interfaces can also lead to blunting and arrest of sinter-cracks, as observed here and elsewhere.[5]

Although the short transverse configuration was expected to be weakest, it exhibited a lower crack growth rate and failed at a higher relative density than did the crack divider configuration, which was expected to be tougher. The images in figure 6 give an indication as to why: stress relief in the short transverse configuration was allowed throughout the sample due to separation of build layers transverse to the loading axis. It can also be seen that stress relief occurred on the other side of the notch where significantly more cracking occurred than in the crack divider sample. In general, the short transverse sample experienced overall greater damage than did the crack divider sample. Thus, the main predictions from Hertzberg are realized here, and it is clear that the crack arrester configuration, with the most available toughening mechanisms, exhibits the greatest toughness.

These results yield another important guideline for design of binder jet printed parts: sinter-cracking may be mitigated ahead of features likely to cause cracking if such features are oriented in the crack arrester configuration during the build. As seen in the previous section, such features include those with a large stress concentration factor or a large cross section with respect to the printed part. Features with lower crack initiation potential may be oriented in the crack divider configuration, while the short transverse configuration should be reserved for those features least likely to cause initiation of sinter-cracks.

Conclusion

This investigation has used in situ monitoring and a uniaxial tension apparatus to shed light on the factors that mitigate sinter-cracking in binder jet printed parts. Conditions were varied on the basis of crack initiator geometry and orientation of the sample with respect to the 3D printing build direction. It was seen that sinter-crack initiation and growth are controlled by both the stress concentration factor of the crack initiating flaw and the size of the flaw with respect to the load-bearing section of the specimen. Initiation requires the flaw to exceed a critical relative size; when the flaw is large enough to initiate cracking, then both the time of initiation and subsequent growth rate depend on the flaw stress concentration factor. Regarding build orientation, sinter-crack initiation and growth were both found to be dependent on the orientation of the flaw with respect to the 3D printing build layers. The crack arrester configuration, in which build layers lie normal to the flaw, was found to give the greatest toughness, experiencing a longer time to initiation and a subsequently slower growth rate. The results of this work show that both

design geometry and build orientation contribute to mitigation of sinter-cracking in binder jet 3D printed parts.

ACKNOWLEDGMENTS

The author is grateful to Prof. Zachary C. Cordero for guiding this work; Mr. Michael D. Bonar for helping to design the experimental method; Ms. Lynnora O. Grant for valuable discussion of the results; Mr. Richard Huff for suggesting the comparison of different build orientations and for encouraging the work; and the Lord Jesus Christ for His grace. The author is further grateful to the National Science Foundation (project number NSF-CMMI-1826064) for funding this work.

References

1. P. Nandwana, A. M. Elliott, D. Siddel, A. Merriman, W. H. Peter, and S. S. Babu, "Powder Bed Binder Jet 3D Printing of Inconel 718: Densification, Microstructural Evolution and Challenges," *Current Opinion in Solid State and Materials Science* 21, no. 4 (2017): 207–218.
2. R. K. Bordia, S.-J. L. Kang, and E. A. Olevsky, "Current Understanding and Future Research Directions at the Onset of the Next Century of Sintering Science and Technology," *Journal of the American Ceramic Society* 100, no. 6 (2017): 2314–2352.
3. T. Rasp, C. Jamin, O. Guillon, and T. Kraft, "Cracking and Shape Deformation of Cylindrical Cavities during Constrained Sintering," *Journal of the European Ceramic Society* 37, no. 8 (2017): 2907–2917.
4. R. K. Bordia and A. Jagota, "Crack Growth and Damage in Constrained Sintering Films," *Journal of the American Ceramic Society* 76, no. 10 (1993): 2475–2485.
5. J. R. Carazzone, M. D. Bonar, H. W. Baring, M. A. Cantu, and Z. C. Cordero, "In Situ Observations of Cracking in Constrained Sintering," *Journal of the American Ceramic Society* 102, no. 2 (2019): 602–610.
6. V. M. Sglavo, P. Z. Cai, and D. J. Green, "Damage in Al2O3 Sintering Compacts under Very Low Tensile Stress," *Journal of Materials Science Letters* 18, no. 11 (1999): 895–900.
7. C. F. Herriott, X. Li, N. Kouraytem, V. Tari, W. Tan, B. Anglin, A. D. Rollett, and A. D. Spear, "A Multi-Scale, Multi-Physics Modeling Framework to Predict Spatial Variation of Properties in Additive-Manufactured Metals," *Modelling and Simulation in Materials Science and Engineering* 27, no. 2 (2019), https://doi.org/10.1088/1361-651X/aaf753
8. W. D. Pilkey, D. F. Pilkey, and R. E. Peterson, *Peterson's Stress Concentration Factors*, 3rd ed. (Hoboken, NJ: Wiley, 2008).
9. J. Schindelin, I. Arganda-Carreras, E. Frise, V. Kaynig, M. Longair, T. Pietzsch, S. Preibisch, et al., "Fiji: An Open-Source Platform for Biological-Image Analysis," *Nature Methods* 9, no. 7 (2012): 676–682.
10. C. P. Ostertag, P. G. Charalambides, and A. G. Evans, "Observations and Analysis of Sintering Damage," *Acta Metallurgica* 37, no. 7 (1989): 2077–2084.
11. J. R. Carazzone, C. L. Martin, and Z. C. Cordero, "Crack Initiation, Propagation, and Arrest in Sintering Powder Aggregates," *Journal of the American Ceramic Society* 103, no. 9 (2020): 4754–4773.
12. T. L. Anderson, *Fracture Mechanics: Fundamentals and Applications*, 3rd ed. (Boca Raton, FL: CRC Press, 2005).

13. A. Jagota and C. Y. Hui, "Mechanics of Sintering Thin Films—II. Cracking Due to Self-Stress," *Mechanics of Materials* 11, no. 3 (1991): 221–234.
14. D. R. Hayhurst, C. J. Morrison, and F. A. Leckie, "The Effect of Stress Concentrations on the Creep Rupture of Tension Panels," *Journal of Applied Mechanics* 42, no. 3 (1975): 613–618.
15. R. W. Hertzberg, *Deformation and Fracture Mechanics of Engineering Materials*, 3rd ed. (New York: Wiley, 1989).
16. L. O. Grant, M. B. Alameen, J. R. Carazzone, C. F. Higgs III, and Z. C. Cordero, "Mitigating Distortion during Sintering of Binder Jet Printed Ceramics," in *Proceedings of the 29th Annual International Solid Freeform Fabrications Symposium—An Additive Manufacturing Conference* (Austin, TX: University of Texas, 2018), 135–142.